



# In-situ synthesis of Ni<sub>2</sub>P co-catalyst decorated Zn<sub>0.5</sub>Cd<sub>0.5</sub>S nanorods for high-quantum-yield photocatalytic hydrogen production under visible light irradiation



Dongsheng Dai<sup>a,b</sup>, Lu Wang<sup>a</sup>, Nan Xiao<sup>b</sup>, Songsong Li<sup>b</sup>, Hao Xu<sup>b</sup>, Shuang Liu<sup>b</sup>, Boran Xu<sup>b</sup>, Da Lv<sup>b</sup>, Yangqing Gao<sup>b</sup>, Weiyu Song<sup>a</sup>, Lei Ge<sup>a,b,\*</sup>, Jian Liu<sup>a,\*</sup>

<sup>a</sup> State Key Laboratory of Heavy Oil Processing, College of Science, China University of Petroleum Beijing, No. 18 Fuxue Rd., Beijing, 102249, People's Republic of China

<sup>b</sup> Department of Materials Science and Engineering, College of Science, China University of Petroleum Beijing, No. 18 Fuxue Rd., Beijing, 102249, People's Republic of China

## ARTICLE INFO

### Keywords:

Photocatalysis

Ni<sub>2</sub>P

Hydrogen evolution

Zn<sub>0.5</sub>Cd<sub>0.5</sub>S

## ABSTRACT

Efficient noble-metal-free semiconductor composite photocatalysts are highly desirable for visible light driven water splitting. In this study, Ni<sub>2</sub>P was successfully decorated on Zn<sub>0.5</sub>Cd<sub>0.5</sub>S as a highly efficient co-catalyst via a hydrothermal method. The chemical as well as photophysical properties of the as-obtained Ni<sub>2</sub>P/Zn<sub>0.5</sub>Cd<sub>0.5</sub>S samples were characterized by X-ray diffractometry (XRD), Transmission electron microscope (TEM), UV-vis diffusion reflectance spectroscopy (DRS), X-ray photoelectron spectroscopy (XPS), photoluminescence (PL) and time-resolved fluorescence. The Ni<sub>2</sub>P/Zn<sub>0.5</sub>Cd<sub>0.5</sub>S composite sample with 4% molar content of Ni<sub>2</sub>P showed the highest photocatalytic H<sub>2</sub> evolution activity with a corresponding H<sub>2</sub> evolution rate of 1173 μmol h<sup>-1</sup>, which was about 13 times higher than that of pure Zn<sub>0.5</sub>Cd<sub>0.5</sub>S sample under visible light irradiation. The photocatalytic activity of the Ni<sub>2</sub>P/Zn<sub>0.5</sub>Cd<sub>0.5</sub>S composite sample was stable even after 4 cycling photocatalytic experiments. A possible mechanism on the photocatalytic enhancement of the Ni<sub>2</sub>P/Zn<sub>0.5</sub>Cd<sub>0.5</sub>S composite sample was systematically investigated, which can provide a novel concept for the synthesis of other desirable semiconductor materials with high photocatalytic performance.

## 1. Introduction

The great advance in the development of human society achieved in last century has also caused tremendous energetic and environmental problems. Benefiting from the Honda-Fujishima effect discovered in 1972 [1], solar driven photocatalytic hydrogen production via water splitting was realized and has been studied extensively as a promising solution to address those issues [2–6]. Various semiconductors such as oxides [7–9], metal sulfides [10–12], and oxynitrides [13,14] have been investigated as potential candidates for efficient photocatalytic H<sub>2</sub> evolution through water splitting. However, none of them meet the needs for practical application, and visible light responsive photocatalyst with excellent charge separation ability and high solution stability still remains as a huge challenge.

Among the various semiconductor photocatalysts which were developed in last decades for photocatalytic H<sub>2</sub> evolution, Zinc cadmium sulfide (Zn<sub>0.5</sub>Cd<sub>0.5</sub>S) has received considerable attention due to its appropriate bandgap and high photocatalytic activity [15–17]. In

addition, Zn<sub>0.5</sub>Cd<sub>0.5</sub>S also exhibits many excellent properties for practical application, including high stability, simple to synthesize and elemental abundant in natural reserves [18,19]. However, its intrinsic drawbacks, in particular low specific surface area, fast charge recombination and narrow light absorption range, have inhibited the further development of Zn<sub>0.5</sub>Cd<sub>0.5</sub>S and should be well addressed. The catalytic activities of Zn<sub>0.5</sub>Cd<sub>0.5</sub>S are determined the morphology and the micro crystal structure [20]. To enhance the photocatalytic activity of Zn<sub>0.5</sub>Cd<sub>0.5</sub>S, loading suitable co-catalysts to capture photo-induced charges and provide rich active sites for surface redox reaction has been demonstrated to be a useful approach. To date, various co-catalysts have been employed to combine with sulfides, including noble metals [21–23], transition metal oxides [24–26], transition metal sulfides [27–29], and hydroxides [30].

However, the most effective major co-catalysts today are predominantly relied on high-cost precious metals which are not suitable for large scale applications [31,32]. Therefore, it is an urgent task to explore the catalytic ability of low-cost non-noble metal co-catalysts for

\* Corresponding authors at: State Key Laboratory of Heavy Oil Processing, College of Science, China University of Petroleum Beijing, No. 18 Fuxue Rd., Beijing, 102249, People's Republic of China.

E-mail addresses: [gelei08@sina.com](mailto:gelei08@sina.com) (L. Ge), [liujian@cup.edu.cn](mailto:liujian@cup.edu.cn) (J. Liu).

photocatalytic hydrogen evolution. Recently, transition-metal phosphides have been studied as co-catalysts, and several groups have shown that transition-metal phosphides, such as Co<sub>2</sub>P [33], Cu<sub>3</sub>P [34,35], CoP [36,37] and FeP [38,39], can be used as co-catalyst to effectively enhance the catalytic performance of photocatalysts. Compare to other noble-metal-free co-catalysts mentioned above, nickel phosphide exhibit many attractive advantages, including high activity of hydrogen production, long term stability [40,41], etc. Therefore nickel phosphides are considered as one of the best alternatives of noble metal co-catalysts.

Motivated by the transition-metal phosphides co-catalysts research mentioned above, herein we prepared one-dimensional Ni<sub>2</sub>P/Zn<sub>0.5</sub>Cd<sub>0.5</sub>S photocatalysts via hydrothermal synthesis method. Detailed characterizations on the morphology, crystal structure, chemical states, and optical properties of the composite photocatalysts were carried out. The photocatalytic H<sub>2</sub> evolution activity and stability of Ni<sub>2</sub>P/Zn<sub>0.5</sub>Cd<sub>0.5</sub>S under visible light irradiation was also characterized. The apparent quantum yield of Ni<sub>2</sub>P/Zn<sub>0.5</sub>Cd<sub>0.5</sub>S for hydrogen production can reach as high as 18.1% at 420 nm. The possible photocatalytic mechanism for enhanced H<sub>2</sub> evolution activity was proposed. Our experimental results demonstrated that Ni<sub>2</sub>P can act as an effective co-catalyst for Zn<sub>0.5</sub>Cd<sub>0.5</sub>S which indicates that it may be also potentially benefiting for other semiconductor photocatalysts for H<sub>2</sub> evolution.

## 2. Experimental

### 2.1. Materials

Zinc acetate dihydrate (Zn(COOCH<sub>3</sub>)<sub>2</sub>·2H<sub>2</sub>O, Aladdin), cadmium acetate dihydrate (Cd(COOCH<sub>3</sub>)<sub>2</sub>·2H<sub>2</sub>O, Aladdin), thioacetamide (A.R.), red phosphorus (A.R.), nickel nitrate (Ni(NO<sub>3</sub>)<sub>2</sub>, A.R.), ethyl alcohol (EtOH, A.R.), ethylenediamine (A.R.), sodium sulfide (A.R.), and sodium thiosulfate (A.R.) were used as received without additional purification or treatment. Deionized water was used in all experiments.

### 2.2. Synthesis of the photocatalysts

The Zn<sub>0.5</sub>Cd<sub>0.5</sub>S sample was prepared according to our previous work with a slight modification [16]. A total of 10 mmol equimolar of zinc acetate dihydrate and cadmium acetate dihydrate were added into 60 ml of ethylenediamine with stirring followed by another addition of 20 mmol thioacetamide. After vigorous stirring for 1 h at room temperature, the white solution was transferred into a 100 ml Teflon-lined stainless steel autoclave. The autoclave was sealed and heated at 180 °C for 24 h. After that, the product was washed by centrifugation with distilled water and ethanol for several times, respectively. Finally, the pure Zn<sub>0.5</sub>Cd<sub>0.5</sub>S sample was obtained via drying the washed solution under vacuum at 60 °C overnight.

The Ni<sub>2</sub>P/Zn<sub>0.5</sub>Cd<sub>0.5</sub>S composites were prepared by hydrothermal method. First, 0.4 g of as-prepared Zn<sub>0.5</sub>Cd<sub>0.5</sub>S sample was dispersed in 60 ml of deionized water under stirring, and then a calculated amount of Ni(NO<sub>3</sub>)<sub>2</sub>·6H<sub>2</sub>O and red phosphorus (the molar ratio of Ni to P is 1:5) were added. The mixture was sonicated for 3 h, then the mixed solution was transferred into a 100 ml Teflon-lined autoclave and heated at 200 °C for 24 h. After that, the products were washed by centrifugation with deionized water and ethanol for three times, respectively. And the final product was obtained by drying the washed solution under vacuum at 60 °C overnight. The molar percentages of Ni<sub>2</sub>P in the prepared composite catalyst were 0%, 0.5%, 1%, 2%, 2.5%, 3%, 4% and 5%, respectively.

### 2.3. Characterization

The X-ray diffractometer (XRD) using Cu K $\alpha$  as radiation was applied to investigate the crystallographic texture of all samples with 2θ range from 20° to 65°. The morphology of all samples was identified by

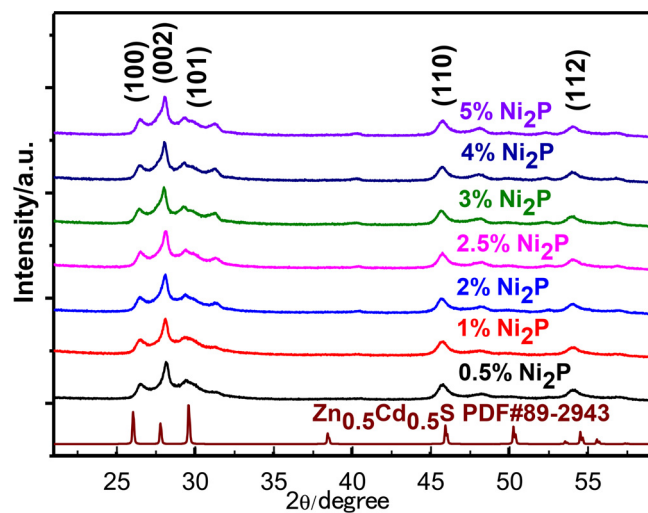


Fig. 1. XRD patterns of Ni<sub>2</sub>P/Zn<sub>0.5</sub>Cd<sub>0.5</sub>S composites with different weight ratios of Ni<sub>2</sub>P.

transmission electron microscopy (TEM, JEM-2100, accelerating voltage 200 kV). The UV-vis diffuse reflection spectroscopy (DRS) of all samples was detected by Shimadzu UV-4100 spectrophotometer, and the reflection from BaSO<sub>4</sub> powder was used as a reflectance standard. X-ray photoelectron spectroscopy (XPS, PHI 5300 ESCA system) was applied to analyze the element valence state of the composite sample, the signal of carbon at 284.8 eV was used as a reference to calibrate the binding energies. The PL spectra of the photocatalysts were detected using a Varian Cary Eclipse spectrometer with an excitation wavelength of 340 nm.

### 2.4. Photocatalytic activity

The photocatalytic H<sub>2</sub> evolution was carried out in a 300 ml quartz reactor (Perfectlight Labsolar IIAG system), which was connected with a low-temperature thermostat bath to keep the reaction temperature at 4 °C during the characterization. The light source (PLS-SXE 300UV Xe arc lamp) was 1 dm over the reactor to illuminate the reactants with light intensity of 11.0 mW/cm<sup>2</sup>. In a typical photocatalytic H<sub>2</sub> evolution experiment, 50 mg of photocatalyst was dispersed in 100 ml of mixed aqueous solution with constant stirring, in which the mixed aqueous solution is composed by 100 ml water and 0.35 M Na<sub>2</sub>S and 0.25 M Na<sub>2</sub>SO<sub>3</sub> as sacrificial reagents. Before each photocatalytic H<sub>2</sub> evolution experiment, the reaction system was evacuated for 30 min to create an anaerobic condition. A gas chromatography (Beifen 3420 A, TCD) was selected to analyze the products, and high purity Argon was utilized as carrier gas.

The apparent quantum yield ( $\phi$ ) for H<sub>2</sub> evolution was determined for the photocatalytic system containing 50 mg 4% Ni<sub>2</sub>P/Zn<sub>0.5</sub>Cd<sub>0.5</sub>S, 0.25 M Na<sub>2</sub>S and 0.35 M Na<sub>2</sub>SO<sub>3</sub> in 100 ml deionized water. The solution was irradiated by 420 nm ( $\pm$  5 nm) visible light irradiation. The apparent quantum efficiency (AQE) could be calculated according to Eq. (1).

$$\text{AQY}(\%) = \frac{\text{the number of reacted electrons}}{\text{the number of incident photons}} \times 100 \quad (1)$$

### 2.5. Density functional theory (DFT) calculation

All calculations were performed using DFT within the plane-wave pseudopotential as implemented in the VASP code with a cutoff energy of 350 eV. The Perdew, Burke, and Ernzerhof (PBE) [42] exchange-correlation functional within a generalized gradient approximation (GGA) was employed. The PAW method was used to describe the effect

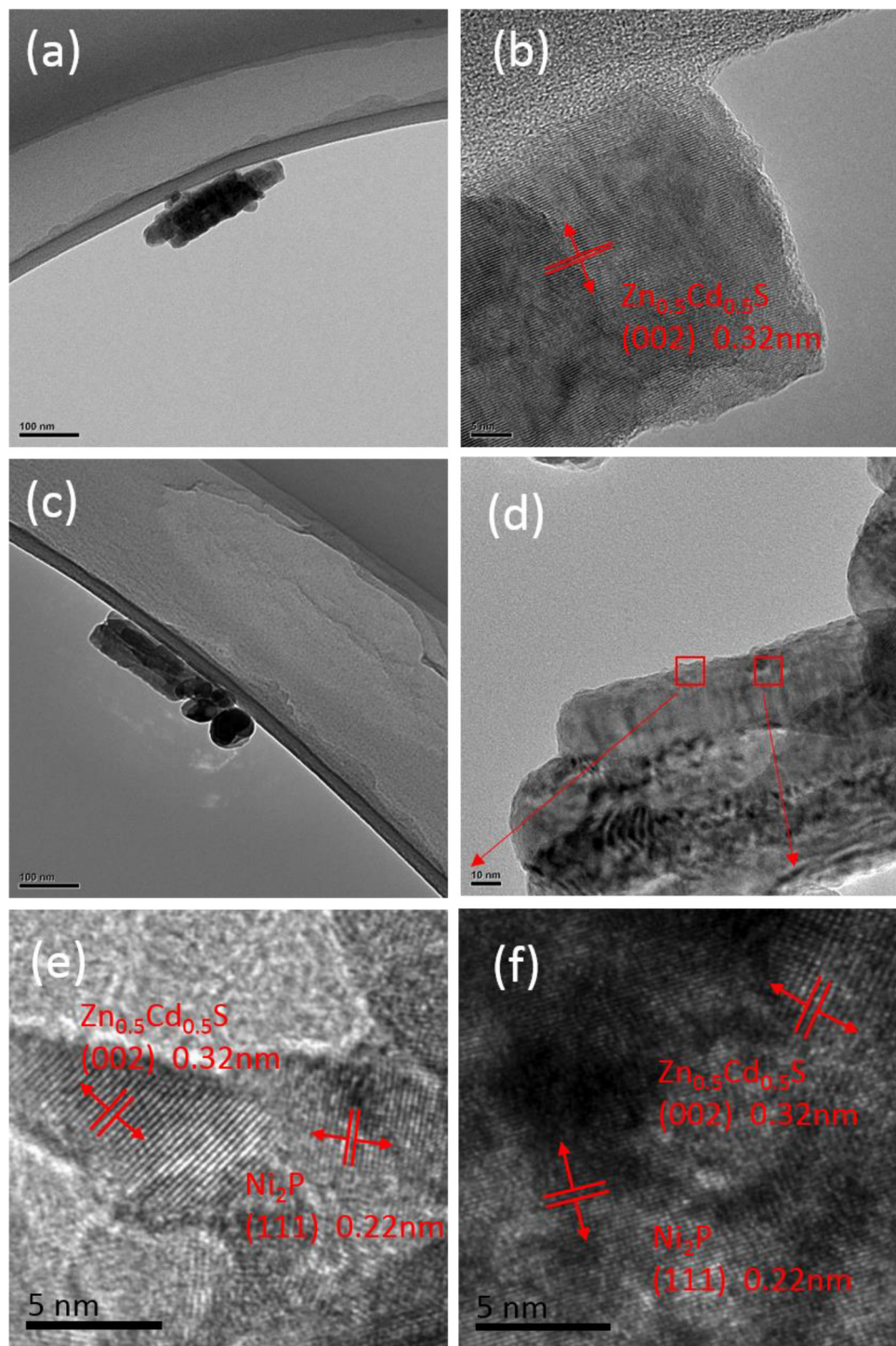


**Fig. 2.** TEM images of  $\text{Zn}_{0.5}\text{Cd}_{0.5}\text{S}$  sample (a),  $\text{Ni}_2\text{P}/\text{Zn}_{0.5}\text{Cd}_{0.5}\text{S}$  composite (c, d); HRTEM image of  $\text{Zn}_{0.5}\text{Cd}_{0.5}\text{S}$  sample (b),  $\text{Ni}_2\text{P}/\text{Zn}_{0.5}\text{Cd}_{0.5}\text{S}$  composite (e, f).

of core electrons [43,44]. Gamma-centered k-point meshes of  $2 \times 2 \times 1$  were used. The atomic positions were relaxed until the force on each atom was less than  $0.05 \text{ eV}/\text{\AA}$ . Using the periodic slab model and self-consistent dipole correction, the averaging electrostatic potential in the planes perpendicular to the slab normal could be obtained.

Bulk  $\text{Zn}_{0.5}\text{Cd}_{0.5}\text{S}$  forms a tetragonal lattice with space group P63mc and experimental lattice constants are:  $a = b = 3.95 \text{ \AA}$ ,  $c = 6.42 \text{ \AA}$ . Bulk  $\text{Ni}_2\text{P}$  forms a tetragonal lattice with space group P-62 m and experimental lattice constants are:  $a = b = 5.86 \text{ \AA}$ ,  $c = 3.38 \text{ \AA}$ . We built a periodic slab with four and four layers for  $\text{Zn}_{0.5}\text{Cd}_{0.5}\text{S}$  (002) and  $\text{Ni}_2\text{P}$  (111) facets, respectively.  $2 \times 2$  and  $1 \times 1$  surface unit cells were used,

respectively. The bottom two layers of  $\text{Zn}_{0.5}\text{Cd}_{0.5}\text{S}$  and  $\text{Ni}_2\text{P}$  are fixed, while the top two layers are relaxed during the calculation. The vacuum gap thickness was set to be  $12 \text{ \AA}$ . The heterostructures are modelled by an interface with  $20 \text{ \AA}$  vacuum to avoid interactions between the adjacent slabs.

### 3. Results and discussion

#### 3.1. Characterization of $\text{Ni}_2\text{P}/\text{Cd}_{0.5}\text{Zn}_{0.5}\text{S}$ composite samples

The phase purity and crystal structure of the as-prepared samples

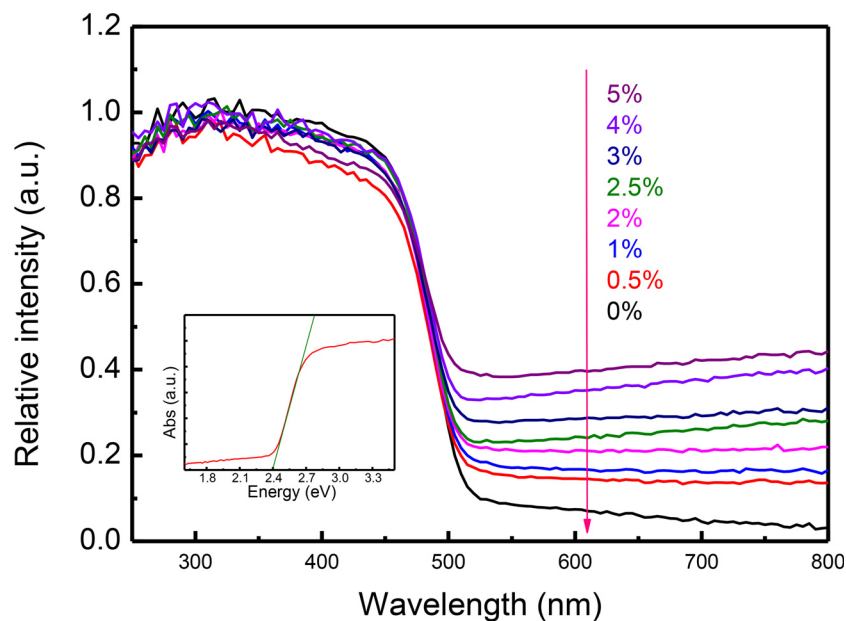


Fig. 3. UV-vis diffuse reflectance spectra of pure Zn<sub>0.5</sub>Cd<sub>0.5</sub>S, and Ni<sub>2</sub>P/Zn<sub>0.5</sub>Cd<sub>0.5</sub>S composites with different molar ratios of Ni<sub>2</sub>P.

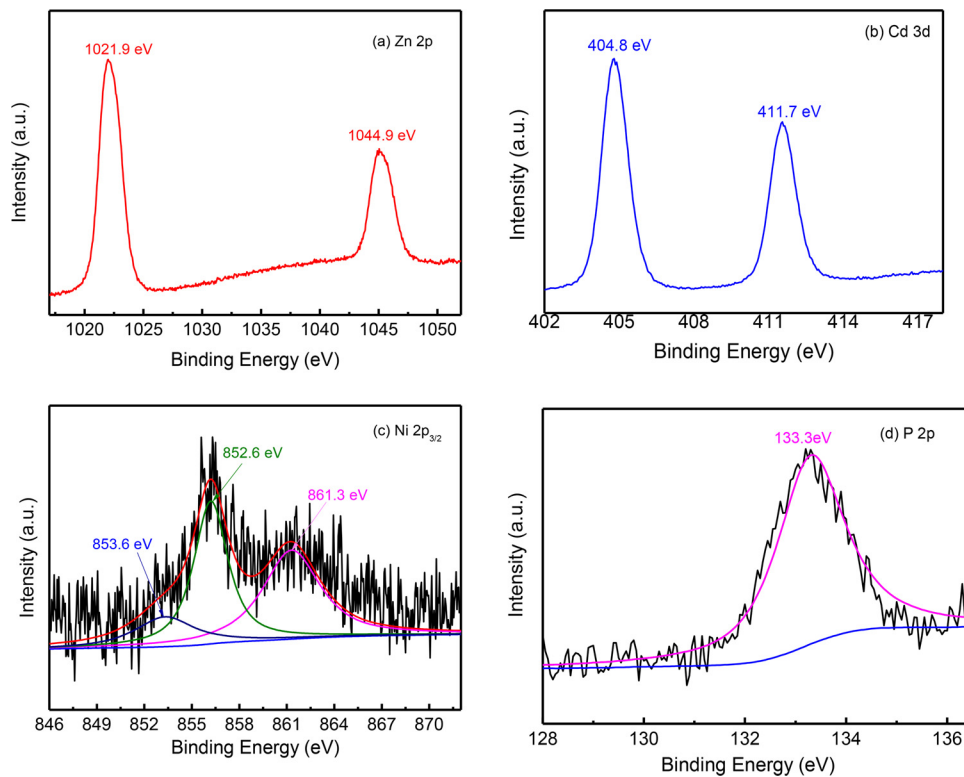
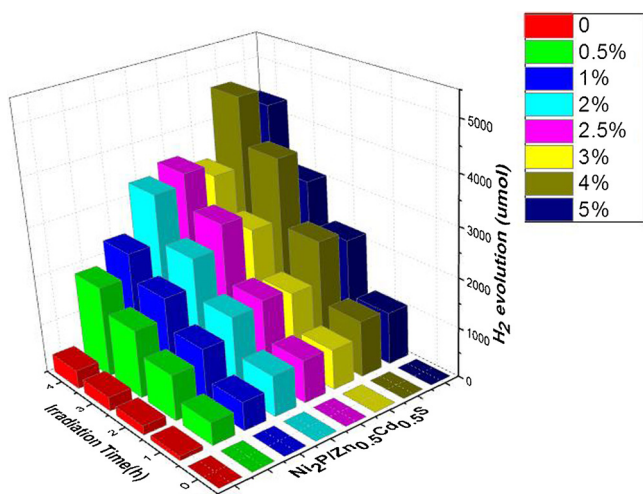


Fig. 4. XPS spectra of Ni<sub>2</sub>P/ Zn<sub>0.5</sub>Cd<sub>0.5</sub>S samples: (a) Zn 2p; (b) Cd 3d; (c) Ni 2p; (d) P 2p.

were determined by XRD analysis. Representative XRD patterns of Ni<sub>2</sub>P/Zn<sub>0.5</sub>Cd<sub>0.5</sub>S are shown in Fig. 1, and the data of the standard card of hexagonal Zn<sub>0.5</sub>Cd<sub>0.5</sub>S (JCPDS No. 89-2943) is also shown as reference. The main peaks of 2θ at 26.11°, 27.76°, 29.62°, 46.02° and 54.58° can be readily indexed to the (100), (002), (101), (110) and (112) planes of hexagonal Zn<sub>0.5</sub>Cd<sub>0.5</sub>S, respectively. It is obvious that the deposition of Ni<sub>2</sub>P did not affect the crystal structure of Zn<sub>0.5</sub>Cd<sub>0.5</sub>S. However, no apparent diffraction peak of Ni<sub>2</sub>P was observed in all composite samples, which may indicates that the deposition content of Ni<sub>2</sub>P in all the Ni<sub>2</sub>P/Zn<sub>0.5</sub>Cd<sub>0.5</sub>S composite samples is quite low which exceeds the sensitive of XRD characterization. Nevertheless, the

presence of Ni<sub>2</sub>P in the composites can be easily proved by TEM and XPS techniques as will be discussed later.

To gain insight into the microstructure details of Ni<sub>2</sub>P/Zn<sub>0.5</sub>Cd<sub>0.5</sub>S, the morphology of the as-prepared samples was characterized by TEM and HRTEM. As shown in Fig. 2 (a), it can be seen that pure Zn<sub>0.5</sub>Cd<sub>0.5</sub>S sample has a rod-like morphology with an average diameter of ~40 nm and length of 100 nm ~ 200 nm. The morphology of Zn<sub>0.5</sub>Cd<sub>0.5</sub>S after the chemical reduction deposition of Ni<sub>2</sub>P is shown in Fig. 2(c), reveals that Ni<sub>2</sub>P was deposited as nanoparticles on the surface of Zn<sub>0.5</sub>Cd<sub>0.5</sub>S with high dispersion, and no other obvious changes in the microstructure of Zn<sub>0.5</sub>Cd<sub>0.5</sub>S nanorods can be found. Fig. 2(b) and Fig. 2(d-f) present the



**Fig. 5.** Photocatalytic  $H_2$  evolution over  $Ni_2P/Zn_{0.5}Cd_{0.5}S$  composite samples with different  $Ni_2P$  contents under visible light.

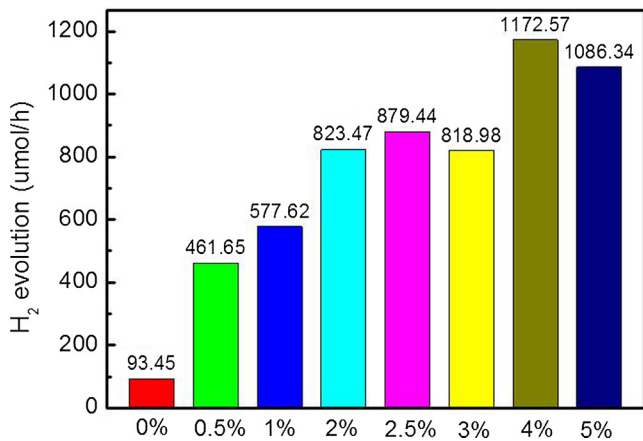


**Fig. 6.** Rate of  $H_2$  evolution over  $Ni_2P/Zn_{0.5}Cd_{0.5}S$  composite samples with different  $Ni_2P$  contents.

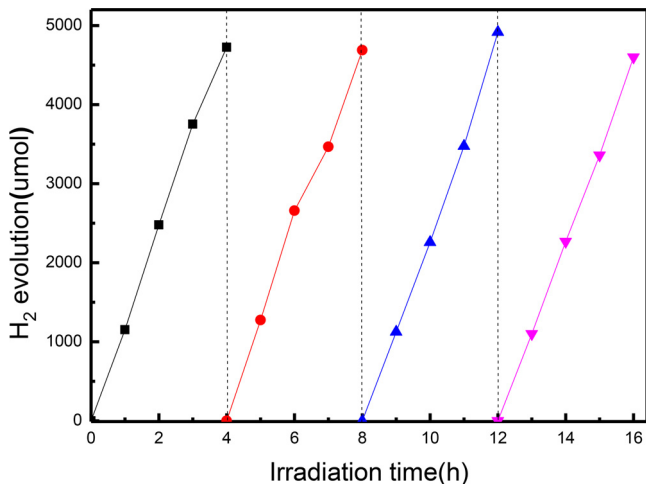


**Fig. 7.** Cycling runs for the photocatalytic  $H_2$  evolution in the presence of the 4%  $Ni_2P/Zn_{0.5}Cd_{0.5}S$  composite sample under visible light irradiation.

HRTEM images of the  $Zn_{0.5}Cd_{0.5}S$  and  $Ni_2P/Zn_{0.5}Cd_{0.5}S$  composite samples, different orientation and interplanar spacing were observed. The identified lattice fringe spacing of 0.32 nm corresponds to the (002) lattice plane of  $Zn_{0.5}Cd_{0.5}S$ . With the deposition of  $Ni_2P$ , a new

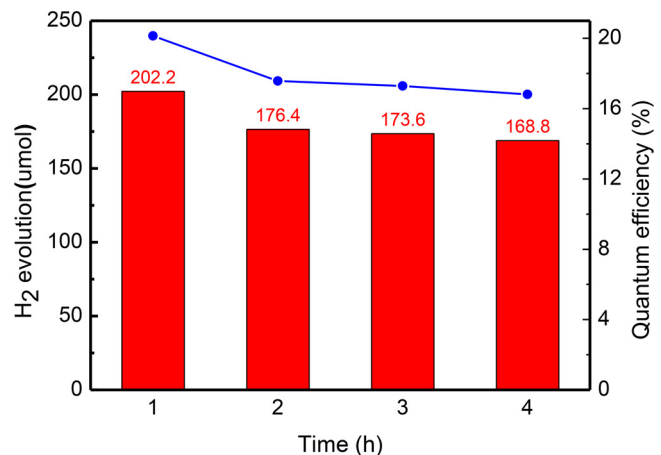


**Fig. 8.** The photocatalytic  $H_2$  evolution and quantum efficiency in the presence of the 4%  $Ni_2P/Zn_{0.5}Cd_{0.5}S$  composite sample under 420 nm light irradiation.

interplanar spacing of 0.22 nm can be seen, which can be ascribed to the (111) lattice plane of  $Ni_2P$  [45]. The TEM and HRTEM characterization results indicate that an intimate contact interface is formed between  $Ni_2P$  and  $Zn_{0.5}Cd_{0.5}S$  components in the  $Ni_2P/Zn_{0.5}Cd_{0.5}S$  composite sample, which could serve as a critical role for effective improvement of the separation efficiency of photo-generated electron-hole pairs.

The UV-vis diffuse reflectance spectra (DRS) of the as-prepared  $Zn_{0.5}Cd_{0.5}S$  and  $Ni_2P/Zn_{0.5}Cd_{0.5}S$  composite samples were performed to characterize their light-absorbing abilities. As shown in Fig. 3, the pure  $Zn_{0.5}Cd_{0.5}S$  sample shows absorption from UV to the visible range with an abrupt decline at  $\sim 500$  nm, which gives an information to its optical band gap. The band gap of  $Zn_{0.5}Cd_{0.5}S$  is determined to be about 2.4 eV by Tauc's plot as shown in the Fig. 3 insert, which is consistent with the value reported previously [46]. After deposition of  $Ni_2P$  co-catalyst, all of the  $Ni_2P/Zn_{0.5}Cd_{0.5}S$  samples have a similar abrupt decline in light absorption at  $\sim 500$  nm, but exhibit a remarkable enhanced light absorption in the visible region compared with pure  $Zn_{0.5}Cd_{0.5}S$ . The absorption intensity of the as-prepared samples in the visible range is strengthened with increasing the deposition content of  $Ni_2P$ , which agrees with the color change of the prepared samples from light yellow to hazel-green. The DRS results demonstrate that the chemical in-situ deposited  $Ni_2P$  has considerable positive influence on the utilization of visible light, and hence the  $Ni_2P/Zn_{0.5}Cd_{0.5}S$  composite sample is expected to have superior photocatalytic performance.

The X-ray photoelectron spectroscopy (XPS) analysis was performed to investigate the surface chemical states of the  $Ni_2P/Zn_{0.5}Cd_{0.5}S$  sample. It can be seen that the binding energy spectrum of Cd shows two peaks at 405.0 and 411.7 eV (Fig. 4a), which are corresponding to Cd 3d<sub>5/2</sub> and Cd 3d<sub>3/2</sub> respectively, indicating that the valence state of Cd element is +2. As shown in Fig. 4b, the binding energies of Zn 2p<sub>3/2</sub> and Zn 2p<sub>1/2</sub> were determined to be 1021.9 and 1044.9 eV, which confirmed the presence of  $Zn^{2+}$ . This result agrees well with the values reported in our previous work [18,19]. Fig. 4c shows the XPS spectrum of Ni 2p<sub>3/2</sub>. The peak at 853.3 eV was assigned to  $Ni^{2+}$  of  $Ni_2P$ , and the other two peaks at 856.2 eV and 861.3 correspond to surface oxidation states [45]. Meanwhile, as shown in Fig. 4d, only one peak at 133.3 eV can be found for the P 2p of  $Ni_2P$  [47,48]. Based on the XPS characterization results, we can conclude that  $Ni_2P$  is successfully deposited on the  $Zn_{0.5}Cd_{0.5}S$  surface.

### 3.2. Photocatalytic $H_2$ evolution activity

The photocatalytic activities of the as-prepared samples were investigated in  $Na_2S$  and  $Na_2SO_3$  aqueous solution under visible-light irradiation and the results are shown in Fig. 5. Control experiment of

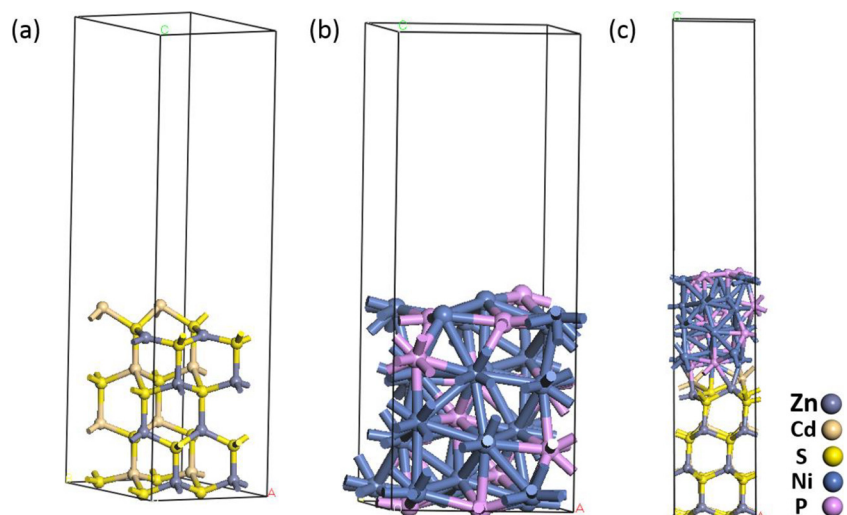


**Fig. 9.** The calculation model for pure samples of  $\text{Zn}_{0.5}\text{Cd}_{0.5}\text{S}$  (a),  $\text{Ni}_2\text{P}$  (b) and the heterojunction metal-semiconductor structure of  $\text{Ni}_2\text{P}/\text{Zn}_{0.5}\text{Cd}_{0.5}\text{S}$  (c).

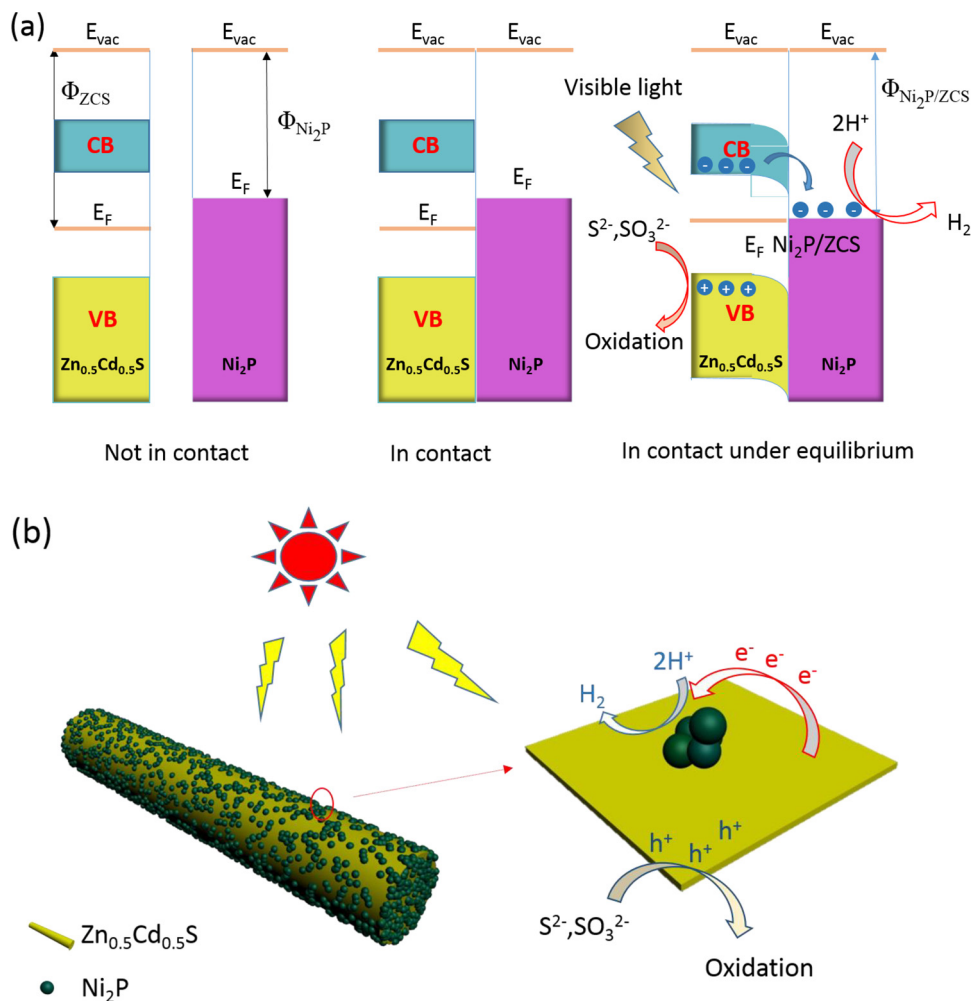


**Fig. 10.** Schematic illustration of charge transfer and  $\text{H}_2$  evolution mechanism of  $\text{Ni}_2\text{P}/\text{Zn}_{0.5}\text{Cd}_{0.5}\text{S}$  under visible light irradiation.

pure  $\text{Ni}_2\text{P}$  sample for  $\text{H}_2$  evolution evaluation is also carried out; the control experiment result shows that pure  $\text{Ni}_2\text{P}$  has no photocatalytic  $\text{H}_2$  evolution activity. The pure  $\text{Zn}_{0.5}\text{Cd}_{0.5}\text{S}$  sample without  $\text{Ni}_2\text{P}$  deposition exhibits a low photocatalytic  $\text{H}_2$  production activity of  $93 \mu\text{mol h}^{-1}$ . After introducing  $\text{Ni}_2\text{P}$ , all of the  $\text{Ni}_2\text{P}/\text{Zn}_{0.5}\text{Cd}_{0.5}\text{S}$  composite samples exhibit a significantly enhanced activity of

photocatalytic hydrogen production. Fig. 6 presents the photocatalytic  $\text{H}_2$  evolution rate of  $\text{Ni}_2\text{P}/\text{Zn}_{0.5}\text{Cd}_{0.5}\text{S}$  composite samples with different  $\text{Ni}_2\text{P}$  deposition contents. After loading 0.5%  $\text{Ni}_2\text{P}$  on  $\text{Zn}_{0.5}\text{Cd}_{0.5}\text{S}$  nanorods, the  $\text{H}_2$  evolution activity is remarkably increased to  $461 \mu\text{mol h}^{-1}$ . Along with increasing the deposition content of  $\text{Ni}_2\text{P}$ , the photocatalytic  $\text{H}_2$  evolution rate is further improved. The 4%  $\text{Ni}_2\text{P}/$

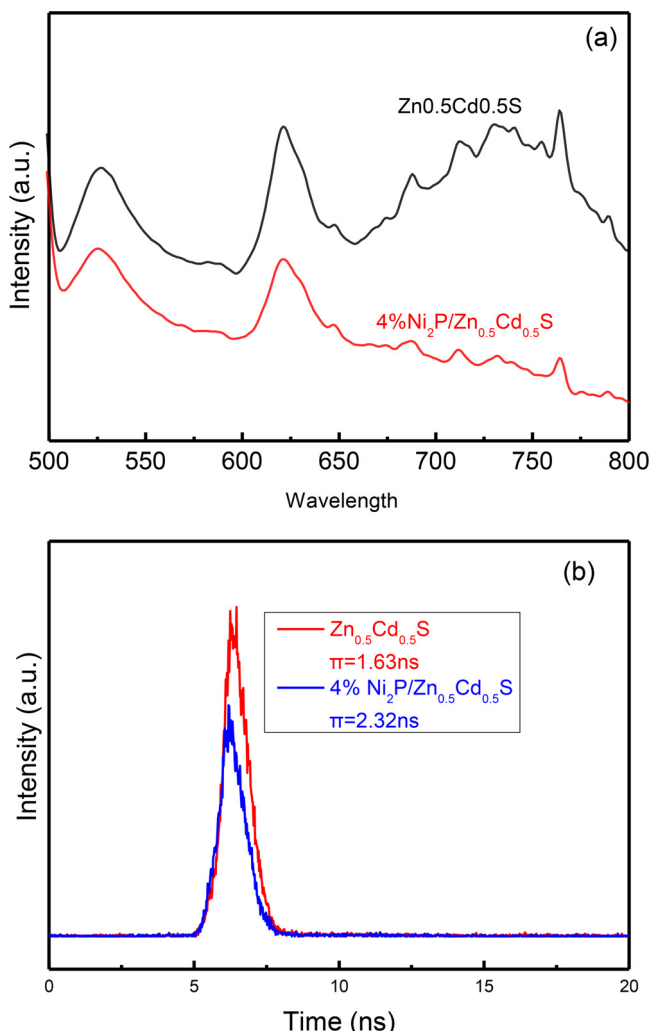


**Fig. 11.** (a) PL spectra of  $\text{Zn}_{0.5}\text{Cd}_{0.5}\text{S}$  and 4%  $\text{Ni}_2\text{P}/\text{Zn}_{0.5}\text{Cd}_{0.5}\text{S}$  samples. (b) The time-resolved fluorescence spectra of  $\text{Zn}_{0.5}\text{Cd}_{0.5}\text{S}$  and 4%  $\text{Ni}_2\text{P}/\text{Zn}_{0.5}\text{Cd}_{0.5}\text{S}$  samples.

$\text{Zn}_{0.5}\text{Cd}_{0.5}\text{S}$  sample presents the highest  $\text{H}_2$  evolution activity with a  $\text{H}_2$  evolution rate of  $1172\text{ umol h}^{-1}$ , which is 13 times higher than that of pure  $\text{Zn}_{0.5}\text{Cd}_{0.5}\text{S}$ . However, further increasing the deposition content of  $\text{Ni}_2\text{P}$  beyond 4% leads to a decrease in photocatalytic  $\text{H}_2$  evolution rate. The decrease in the photocatalytic activity may be due to the high loading ratio of black  $\text{Ni}_2\text{P}$ , which would inhibit the light absorption of  $\text{Zn}_{0.5}\text{Cd}_{0.5}\text{S}$ , leading to a reduction in the number of photo generated carriers. Thus, the competition of light absorption between  $\text{Ni}_2\text{P}$  and  $\text{Zn}_{0.5}\text{Cd}_{0.5}\text{S}$  should be the key parameter for the deterioration in photocatalytic  $\text{H}_2$  evolution rate. Therefore, a suitable loading amount of  $\text{Ni}_2\text{P}$  is important for the optimization of the photocatalytic activity of  $\text{Ni}_2\text{P}/\text{Zn}_{0.5}\text{Cd}_{0.5}\text{S}$  composite samples.

The stability of a photocatalyst is highly critical for practical applications. To investigate the durability of the  $\text{Ni}_2\text{P}/\text{Zn}_{0.5}\text{Cd}_{0.5}\text{S}$  photocatalyst, the photocatalytic activity of the 4%  $\text{Ni}_2\text{P}/\text{Zn}_{0.5}\text{Cd}_{0.5}\text{S}$  sample was investigated via cycling test of photocatalytic  $\text{H}_2$  evolution experiments. Fig. 7 illustrates the  $\text{H}_2$  evolution curves in cycling photocatalytic run. The  $\text{H}_2$  production rate does not display obvious decrease after being irradiated for 16 h (4 cycles), which indicates that the 4%  $\text{Ni}_2\text{P}/\text{Zn}_{0.5}\text{Cd}_{0.5}\text{S}$  photocatalyst has sufficient stability for photocatalytic  $\text{H}_2$  production.

Moreover, in order to further evaluate the photocatalytic activity of  $\text{Ni}_2\text{P}/\text{Zn}_{0.5}\text{Cd}_{0.5}\text{S}$ , its apparent quantum yield was measured at  $420\text{ nm}$  ( $\pm 5\text{ nm}$ ). One molecule of  $\text{H}_2$  is assumed to be generated by the

absorption of two photons. The result of apparent quantum yield is shown in Fig. 8. The average rate of  $\text{H}_2$  evolution is  $\sim 202\text{ }\mu\text{mol h}^{-1}$  which sets  $\phi$  to be 18.95%. This high apparent quantum yield for photocatalytic  $\text{H}_2$  evolution stands for an efficient conversion of visible light energy, suggesting that the  $\text{Ni}_2\text{P}/\text{Zn}_{0.5}\text{Cd}_{0.5}\text{S}$  composite photocatalyst is highly active for electron-hole pair generation and separation. Thus, it can be seen that  $\text{Ni}_2\text{P}/\text{Zn}_{0.5}\text{Cd}_{0.5}\text{S}$  is an efficient photocatalyst for visible-light-driven photocatalytic  $\text{H}_2$  evolution.

### 3.3. Photocatalytic mechanism investigation

It is important to clarify the underlying reason for the significant improvement in the photocatalytic  $\text{H}_2$  evolution performance of these  $\text{Ni}_2\text{P}$  modified  $\text{Zn}_{0.5}\text{Cd}_{0.5}\text{S}$  samples. We then calculated the work function of the materials via preliminary density functional theory (DFT) to reveal the charge injection behaviors at the  $\text{Ni}_2\text{P}/\text{Zn}_{0.5}\text{Cd}_{0.5}\text{S}$  interface. The calculation model of  $\text{Zn}_{0.5}\text{Cd}_{0.5}\text{S}$  (002),  $\text{Ni}_2\text{P}$  (111) and the heterojunction metal-semiconductor structure of  $\text{Zn}_{0.5}\text{Cd}_{0.5}\text{S}$  (002)/ $\text{Ni}_2\text{P}$  (111) is shown in Fig. 9(a, b, c). In this system, the work functions of the metallic  $\text{Ni}_2\text{P}$  (111) and  $\text{Zn}_{0.5}\text{Cd}_{0.5}\text{S}$  (002) are 4.94 eV and 6.78 eV, respectively. As is well-known, different work function of metal and semiconductor will results in energy band bending when they are bring into intimate contact [49,50]. Therefore, when  $\text{Zn}_{0.5}\text{Cd}_{0.5}\text{S}$  and  $\text{Ni}_2\text{P}$  form intimate contact, the electrons will transfer from  $\text{Ni}_2\text{P}$  to  $\text{Zn}_{0.5}\text{Cd}_{0.5}\text{S}$  as the Fermi level of  $\text{Ni}_2\text{P}$  is higher than  $\text{Zn}_{0.5}\text{Cd}_{0.5}\text{S}$ , and leading to a downward energy band bending at the  $\text{Ni}_2\text{P}/\text{Zn}_{0.5}\text{Cd}_{0.5}\text{S}$  interface. After the electronic equilibrium of the heterojunction system is reached, the unified work function was observed to be 6.02 eV.

Based on the calculation of work function and the photocatalytic  $\text{H}_2$  evolution performance of  $\text{Ni}_2\text{P}/\text{Zn}_{0.5}\text{Cd}_{0.5}\text{S}$ , a possible mechanism for the enhanced photocatalytic  $\text{H}_2$  evolution activity of the  $\text{Ni}_2\text{P}/\text{Zn}_{0.5}\text{Cd}_{0.5}\text{S}$  photocatalyst is proposed. As depicted in Fig. 10(a, b),  $\text{Zn}_{0.5}\text{Cd}_{0.5}\text{S}$  absorbs photons and generates electron-hole pairs under visible-light irradiation. However, without the deposition of  $\text{Ni}_2\text{P}$  cocatalyst, the photo-generated electrons and holes are likely to recombine rapidly which leads to a low photocatalytic  $\text{H}_2$  production activity. After depositing  $\text{Ni}_2\text{P}$  on the surface of  $\text{Zn}_{0.5}\text{Cd}_{0.5}\text{S}$ , the photo-induced electron will transfer rapidly from  $\text{Zn}_{0.5}\text{Cd}_{0.5}\text{S}$  to  $\text{Ni}_2\text{P}$  due to the strong internal potential field formed at the  $\text{Ni}_2\text{P}/\text{Zn}_{0.5}\text{Cd}_{0.5}\text{S}$  interface, and then reduce  $\text{H}^+$  to  $\text{H}_2$  via the active sites present at the surface of  $\text{Ni}_2\text{P}$ . The photo-induced holes will be accumulated on the surface of  $\text{Zn}_{0.5}\text{Cd}_{0.5}\text{S}$  and are consumed by  $\text{Na}_2\text{S}$  and  $\text{Na}_2\text{SO}_3$  sacrificial regents [18,50]. As a consequence, the  $\text{Ni}_2\text{P}$  can act as an electron collector and transporter to prolong the lifetime of the charge carriers, thus improving the photocatalytic activity of the  $\text{Ni}_2\text{P}/\text{Zn}_{0.5}\text{Cd}_{0.5}\text{S}$  samples.

To verify the proposed mechanism for the enhanced photocatalytic performance in the  $\text{Ni}_2\text{P}$  composite sample, photoluminescence (PL) spectra of pure  $\text{Zn}_{0.5}\text{Cd}_{0.5}\text{S}$  and 4%  $\text{Ni}_2\text{P}/\text{Zn}_{0.5}\text{Cd}_{0.5}\text{S}$  composite sample were obtained to probe the status of radiative recombination of the photo-generated charge carriers. A high recombination rate of excited holes and electrons in the photocatalyst generally results in a low photocatalytic activity [4]. As shown in Fig. 11(a), it was found that the PL intensity of 4%  $\text{Ni}_2\text{P}/\text{Zn}_{0.5}\text{Cd}_{0.5}\text{S}$  is lower than the pure  $\text{Zn}_{0.5}\text{Cd}_{0.5}\text{S}$ . The results clearly indicate that the presence of  $\text{Ni}_2\text{P}$  is favorable for suppressing the recombination process of electron-holes, leading to high photocatalytic hydrogen production activity. Therefore, a noticeable enhancement in the photocatalytic activity is achieved in the  $\text{Ni}_2\text{P}/\text{Zn}_{0.5}\text{Cd}_{0.5}\text{S}$  composite sample. The PL results fitted well with the energy band analysis result and photocatalytic activity characterization of the samples. To give a further evidence for the proposed photocatalytic mechanism, the dynamic behavior of photo-generated charge carriers was also investigated with the assistance of time-resolved fluorescence spectroscopy (Fig. 11(b)). It can be seen that the PL decay lifetime of the photocatalyst increases in the order of  $\text{Zn}_{0.5}\text{Cd}_{0.5}\text{S} < \text{Ni}_2\text{P}/\text{Zn}_{0.5}\text{Cd}_{0.5}\text{S}$ , and the lifetime was determined to be 1.63 ns and 2.32 ns,

respectively. The time-resolved fluorescence result clearly confirm that the recombination of photogenerated charge carriers is indeed suppressed in the Ni<sub>2</sub>P/Zn<sub>0.5</sub>Cd<sub>0.5</sub>S nanorod samples.

#### 4. Conclusions

In summary, a highly efficient composite and noble-metal-free photocatalyst Ni<sub>2</sub>P/Zn<sub>0.5</sub>Cd<sub>0.5</sub>S was prepared via hydrothermal method. The Ni<sub>2</sub>P NPs are dispersed uniformly on the surface of Zn<sub>0.5</sub>Cd<sub>0.5</sub>S nanorods and form intimate contact interfaces. A highest H<sub>2</sub> amount as high as 1172 μmol h<sup>-1</sup> was obtained in 4% Ni<sub>2</sub>P/Zn<sub>0.5</sub>Cd<sub>0.5</sub>S sample, which is 13 times than that of pure Zn<sub>0.5</sub>Cd<sub>0.5</sub>S. In addition, the 4% Ni<sub>2</sub>P/Zn<sub>0.5</sub>Cd<sub>0.5</sub>S sample also exhibited a good stability in the cycling photocatalytic experiments. Finally, combined with the DFT calculation result of the Ni<sub>2</sub>P/Zn<sub>0.5</sub>Cd<sub>0.5</sub>S heterojunction structure, a possible photocatalytic mechanism is proposed to explain the observed H<sub>2</sub> evolution activity enhancement in the Ni<sub>2</sub>P decorated Zn<sub>0.5</sub>Cd<sub>0.5</sub>S sample, which was further confirmed by photoluminescence (PL) and time-resolved fluorescence characterizations. Therefore, our experimental results demonstrated that Ni<sub>2</sub>P is a promising co-catalyst for Zn<sub>0.5</sub>Cd<sub>0.5</sub>S, which can also be regarded as potential functional co-catalyst to promote the photocatalytic H<sub>2</sub> production activity of other semiconductor photocatalysts.

#### Acknowledgements

This work was financially supported by the National Science Foundation of China (Grant No. 51572295, 21273285 and 21003157), Beijing Nova Program (Grant No. 2008B76), and Science Foundation of China University of Petroleum, Beijing (Grant No. KYJJ2012-06-20 and 2462016YXBS05).

#### References

- [1] A. Fujishima, K. Honda, *Nature* 238 (1972) 37–38.
- [2] X. Feng, S. Maier, M. Salmeron, *J. Am. Chem. Soc.* 134 (2012) 5662–5668.
- [3] M.R. Hoffmann, S.T. Martin, W. Choi, D.W. Bahnemann, *Chem. Rev.* 95 (1995) 69–96.
- [4] A. Kudo, Y. Miseki, *Chem. Soc. Rev.* 38 (2009) 253–278.
- [5] R.-B. Wei, Z.-L. Huang, G.-H. Gu, Z. Wang, L. Zeng, Y. Chen, Z.-Q. Liu, *Appl. Catal. B Environ.* 231 (2018) 101–107.
- [6] S. Ma, Y. Deng, J. Xie, K. He, W. Liu, X. Chen, X. Li, *Appl. Catal. B Environ.* 227 (2018) 218–228.
- [7] H. Mou, C. Song, Y. Zhou, B. Zhang, D. Wang, *Appl. Catal. B Environ.* 221 (2018) 565–573.
- [8] H. Xu, S. Li, L. Ge, C. Han, Y. Gao, D. Dai, *Int. J. Hydrogen Energy* 42 (2017) 22877–22886.
- [9] S. Fang, Y. Xin, L. Ge, C. Han, P. Qiu, L. Wu, *Appl. Catal. B Environ.* 179 (2015) 458–467.
- [10] S. Li, D. Dai, L. Ge, Y. Gao, C. Han, N. Xiao, *Dalton Trans.* 46 (2017) 10620–10629.
- [11] X. Fu, L. Zhang, L. Liu, H. Li, S. Meng, X. Ye, S. Chen, *J. Phys. Chem. A* 5 (2017) 15287–15293.
- [12] X. Hao, Y. Wang, J. Zhou, Z. Cui, Y. Wang, Z. Zou, *Appl. Catal. B Environ.* 221 (2018) 302–311.
- [13] L.J. Zhang, S. Li, B.K. Liu, D.J. Wang, T.F. Xie, *Acc Catal.* 4 (2014) 3724–3729.
- [14] L. Pei, Z. Xu, S. Yan, Z. Zou, *J. Phys. Chem. A* 5 (2017) 12848–12855.
- [15] J. Fu, B. Zhu, W. You, M. Jaroniec, J. Yu, *Appl. Catal. B Environ.* 220 (2018) 148–160.
- [16] Z. Mei, B. Zhang, J. Zheng, S. Yuan, Z. Zhuo, X. Meng, Z. Chen, K. Amine, W. Yang, L.W. Wang, W. Wang, S. Wang, Q. Gong, J. Li, F.S. Liu, F. Pan, *Nano Energy* 26 (2016) 405–416.
- [17] J. Song, H. Zhao, R. Sun, X. Li, D. Sun, *Energy Environ. Sci.* 10 (2017) 225–235.
- [18] D. Dai, H. Xu, L. Ge, C. Han, Y. Gao, S. Li, Y. Lu, *Appl. Catal. B Environ.* 217 (2017) 429–436.
- [19] L. Wu, J. Gong, L. Ge, C. Han, S. Fang, Y. Xin, Y. Li, Y. Lu, *Int. J. Hydrogen. Energy* 41 (2016) 14704–14712.
- [20] Y. Wang, J. Wu, J. Zheng, R. Xu, *Catal. Sci. Technol.* 1 (2011) 940–947.
- [21] G. Han, Y.-H. Jin, R.A. Burgess, N.E. Dickenson, X.-M. Cao, Y. Sun, *J. Am. Chem. Soc.* 139 (2017) 15584–15587.
- [22] P. Du, R. Eisenberg, *Energy Environ. Sci.* 5 (2012) 6012–6021.
- [23] P.Y. Kuang, P.X. Zheng, Z.Q. Liu, J.L. Lei, H. Wu, N. Li, T.Y. Ma, *Small* 12 (2016) 6735–6744.
- [24] R.-B. Wei, P.-Y. Kuang, H. Cheng, Y.-B. Chen, J.-Y. Long, M.-Y. Zhang, Z.-Q. Liu, *ACS Sustain. Chem. Eng.* 5 (2017) 4249–4257.
- [25] J. Liu, Q. Jia, J. Long, X. Wang, Z. Gao, Q. Gu, *Appl. Catal. B Environ.* 222 (2018) 35–43.
- [26] P.-Y. Kuang, Y.-Z. Su, K. Xiao, Z.-Q. Liu, N. Li, H.-J. Wang, J. Zhang, *ACS Appl. Mater. Interfaces* 7 (2015) 16387–16394.
- [27] S. Ma, X. Xu, J. Xie, X. Li, *Chin. J. Catal.* 38 (2017) 1970–1980.
- [28] Y. Chao, J. Zheng, J. Chen, Z. Wang, S. Jia, H. Zhang, Z. Zhu, *Catal. Sci. Technol.* 7 (2017) 2798–2804.
- [29] J. Yu, J. Zhang, M. Jaroniec, *Green Chem.* 12 (2010) 1611–1614.
- [30] J. Yu, S. Wang, B. Cheng, Z. Lin, F. Huang, *Catal. Sci. Technol.* 3 (2013) 1782–1789.
- [31] Y.A. Attia, D. Buceta, C. Blanco-Varela, M.B. Mohamed, G. Barone, M.A. López-Quintela, *J. Am. Chem. Soc.* 136 (2014) 1182–1185.
- [32] X. Li, S. Fang, L. Ge, C. Han, P. Qiu, W. Liu, *Appl. Catal. B Environ.* 176–177 (2015) 62–69.
- [33] C. Huang, T. Ouyang, Y. Zou, N. Li, Z.-Q. Liu, *J. Phys. Chem. A* (2018).
- [34] X. Yue, S. Yi, R. Wang, Z. Zhang, S. Qiu, *Nanoscale* 8 (2016) 17516–17523.
- [35] Y. Wang, J. Wu, J. Zheng, R. Xu, *Catal. Sci. Technol.* 1 (2011) 940–947.
- [36] Y. Peng, L. Wang, Y. Liu, H. Chen, J. Lei, J. Zhang, *Eur. J. Inor. Chem.* 2017 (2017) 4797–4802.
- [37] D. Zhao, B. Sun, X. Li, L. Qin, S. Kang, D. Wang, *RSC Adv.* 6 (2016) 33120–33125.
- [38] S. Cao, Y. Chen, C.-J. Wang, X.-J. Lv, W.-F. Fu, *Chem. Commun.* 51 (2015) 8708–8711.
- [39] H. Cheng, X.-J. Lv, S. Cao, Z.-Y. Zhao, Y. Chen, W.-F. Fu, *Sci. Rep.* 6 (2016) 19846.
- [40] W. Zhen, X. Ning, B. Yang, Y. Wu, Z. Li, G. Lu, *Appl. Catal. B Environ.* 221 (2018) 243–257.
- [41] J. Tian, Q. Liu, Y. Liang, Z. Xing, A.M. Asiri, X. Sun, *ACS Appl. Mater. Interfaces* 6 (2014) 20579–20584.
- [42] J.P. Perdew, K. Burke, M. Ernzerhof, *Phys. Rev. Lett.* 77 (1996) 3865–3868.
- [43] P.E. Blöchl, *Phys. Rev. B* 50 (1994) 17953–17979.
- [44] G. Kresse, D. Joubert, From ultrasoft pseudopotentials to the projector augmented-wave method, *Phys. Rev. B* 59 (1999) 1758–1775.
- [45] Z. Qin, F. Xue, Y. Chen, S. Shen, L. Guo, *Appl. Catal. B Environ.* 217 (2017) 551–559.
- [46] Q. Li, H. Meng, P. Zhou, Y. Zheng, J. Wang, J. Yu, J. Gong, *ACS Catal.* 3 (2013) 882–889.
- [47] Y. Wang, Y. Wang, R. Jiang, R. Xu, *Ind. Eng. Chem. Res.* 51 (2012) 9945–9951.
- [48] X. Liu, X. Li, L. Qin, J. Mu, S.-Z. Kang, *J. Mater. Chem. A* 5 (2017) 14682–14688.
- [49] S. Bai, J. Jiang, Q. Zhang, Y. Xiong, *Chem. Soc. Rev.* 44 (2015) 2893–2939.
- [50] X. Yue, S. Yi, R. Wang, Z. Zhang, S. Qiu, *Appl. Catal. B Environ.* 224 (2018) 17–26.